Acta Pharmaceutica Sinica B 2015;5(1):25–33

HOSTED BY

ELSEVIER

Chinese Pharmaceutical Association
Institute of Materia Medica, Chinese Academy of Medical Sciences

Acta Pharmaceutica Sinica B

www.elsevier.com/locate/apsb
www.sciencedirect.com

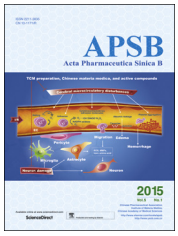

REVIEW

Near-infrared fluorescent probes for imaging of amyloid plaques in Alzheimer's disease

Hongjuan Tong[a], **Kaiyan Lou**[a,*], **Wei Wang**[a,b,**]

[a]*Shanghai Key Laboratory of Chemical Biology, School of Pharmacy, State Key Laboratory of Bioengineering Reactor, East China University of Science and Technology, Shanghai 200237, China*
[b]*Department of Chemistry and Chemical Biology, University of New Mexico, Albuquerque, NM 87131-0001, USA*

Received 16 November 2014; received in revised form 8 December 2014; accepted 11 December 2014

KEY WORDS

Alzheimer's disease;
Blood-brain barrier;
Fluorescence probe;
Near-infrared fluorescence;
Optical imaging;
Amyloid-β plagues

Abstract One of the early pathological hallmarks of Alzheimer's disease (AD) is the deposition of amyloid-β (Aβ) plaques in the brain. There has been a tremendous interest in the development of Aβ plaques imaging probes for early diagnosis of AD in the past decades. Optical imaging, particularly near-infrared fluorescence (NIRF) imaging, has emerged as a safe, low cost, real-time, and widely available technique, providing an attractive approach for *in vivo* detection of Aβ plaques among many different imaging techniques. In this review, we provide a brief overview of the state-of-the-art development of NIRF Aβ probes and their *in vitro* and *in vivo* applications with special focus on design strategies and optical, binding, and brain-kinetic properties.

Abbreviations: Aβ, amyloid-β; Ach, acetylcholine; AD, Alzheimer's disease; APP, amyloid peptide precursor; BAP, BODIPY-based Ab imaging probe; BBB, blood-brain barrier; Cy, cyanine dyes; ICG, indocyanine green dyes; MRI, magnetic resonance imaging; NIR, near-infrared; NIRF, near-infrared fluorescence; PET, positron emission tomography; ROS, reactive oxygen species; SPECT, single photon emission computed tomography

*Corresponding author. Tel./fax: +86 21 64253299.
**Corresponding author at: Department of Chemistry and Chemical Biology, University of New Mexico, Albuquerque, NM 87131-0001, USA. Tel.: +1 505 2770756; fax: +1 505 2772609.
E-mail addresses: kylou@ecust.edu.cn (Kaiyan Lou), wwang@unm.edu (Wei Wang).

Peer review under responsibility of Institute of Materia Medica, Chinese Academy of Medical Sciences and Chinese Pharmaceutical Association.

http://dx.doi.org/10.1016/j.apsb.2014.12.006

1. Introduction

Alzheimer's disease (AD) is the most common type of dementia among older people, affecting approximately 35 million people worldwide, with 5 million new cases every year[1]. Clinical symptoms of AD include progressive cognitive decline, irreversible memory loss, disorientation, language impairment, and emotional instability[1]. The dilemma places significant mental, social and economic burdens on patients, families, and communities[1]. Unfortunately, there are no currently effective treatments available to reverse or stop the progress of this devastating disease, primarily due to difficulties in identification of disease etiology[2–4].

Several pathological hallmarks of this disease have been identified, namely, the deposition of amyloid-β (Aβ) plaques and neurofibrillary tangles, elevated reactive oxygen species (ROS), imbalanced metal ion (*e.g.*, Cu, Fe, and Zn) homeostasis, and decreased brain acetylcholine (Ach) levels. Three major theories have been proposed to explain these pathological hallmarks: amyloid cascade[3,5,6], oxidative stress[7,8], and the metal ion hypotheses[7]. The amyloid cascade hypothesis is currently the prevailing one. It is believed that the formation Aβ plaques arises from aggregation of peptides Aβ_{40} and Aβ_{42}, and is the initial event in the pathogenesis of the AD. Aβ_{40} and Aβ_{42} are degradation products of amyloid peptide precursor (APP), generated from cleavage by β- and γ-secretases. These cleaved peptides have a tendency to aggregate into different Aβ species such as dimers, oligomers, fibrils, and plaques, and may also interact with metal ions and produce ROS, with subsequent neuronal atrophy and death[4]. Regardless of the nature of the intertwined toxicological pathways induced by Aβ aggregates, it is widely accepted that the formation of Aβ plaques precedes the clinical symptoms of AD. Therefore, they are excellent diagnostic and predictive biomarkers for the early detection of AD[5,6,9]. Moreover, the current clinical diagnosis of AD is primarily based upon family and patient's medical history as well as neurological and neuropsychological observations. Thus, the diagnosis is often inaccurate. Confirmative AD diagnosis can only be made through postmortem histopathological examination of brain Aβ plaques. There exists a great and urgent need to develop non-invasive and accurate probes for Aβ plaques to improve the current diagnosis of AD. Such probes will also be useful in monitoring disease progression and effectiveness of new AD treatments.

In the past decade, significant advances have been made in the design of molecular probes for specific labeling, detection, imaging of Aβ plaques both *in vitro* and *in vivo*. A number of different imaging modalities and approaches have been applied, including magnetic resonance imaging (MRI)[10–14], positron emission tomography (PET)[15–19], single photon emission computed tomography (SPECT)[20–24], and optical imaging techniques[25]. MRI based approaches suffer from low resolution since the size of Aβ plaques typically range from 20 to 60 μm, while only larger plaques (>50 μm) are detectable[26]. Compared with MRI, radiolabeled PET and SPECT probes are more sensitive methods. Many probes, such as [^{11}C]PIB[27,28], [^{11}C]SB-13[29,30], [^{11}C]AZD2184[31], [^{18}F]FPIB[32], [^{18}F]AZD4694[33,34], [^{18}F]FDDNP[35,36], [^{18}F]AV-1[37-39], [^{18}F]AV-45[40–42] and [^{123}I]IMPY[20], have advanced in clinical trials. PET-based probes are more promising in terms of their translational applications. Three PET probes [^{18}F]FPIB (Vizamyl^{TM}), [^{18}F]AV-45 (Amyvid^{TM}) and [^{18}F]AV-1 (Neuraceq^{TM}) were recently approved by the FDA. The clinical diagnostic utility of these PET imaging agents is limited: they cannot be used to confirmatively diagnose AD, only to support other diagnostic criteria[43]. Furthermore, the use of PET probes is limited by high cost and narrow availability, since generation of these probes needs specialized facilities that have a cyclotron for the generation of short-lived radionuclides (*e.g.*, [^{11}C], $t_{1/2}$=20 min and [^{18}F], $t_{1/2}$=110 min) and an automated synthetic unit to produce radiolabelled probes. Compared with PET, SPECT has broader availability and lower cost as a routine diagnosis method due to the use of easily-generated radionuclides with longer half-lives (*e.g.*, [^{125}I], $t_{1/2}$=60.1 d, [^{123}I], $t_{1/2}$=13.2 h, and [^{99m}Tc], $t_{1/2}$=6.0 h). Current SPECT-based probes either have relatively high background for the radioiodinated probes due to high lipophilicity and nonspecific binding or have poor blood-brain barrier (BBB) penetration in the case of ^{99m}Tc-labeled SPECT probes. Only one SPECT probe, [^{123}I]IMPY, has advanced in clinical trials. In general, radionuclear-based imaging modalities PET and SPECT are limited by high cost, radiation exposure, and single signal readout.

In contrast to the radionuclear-based imaging techniques, optical imaging modalities are rather inexpensive; important merits include nonradioactive, real-time imaging with the option of multi-targets tracing *in vitro* and *in vivo*, wide availability, and high-resolution imaging depending on the specific technique used[44–47]. For *in vivo* applications, in order to avoid absorption and background autofluorescence and scattering of biological molecules, probe fluorescence emission wavelength in the near-infrared (NIR) region between 650 and 900 nm is advantageous so that one can achieve an optimal penetration depth and high sensitivity. Therefore, NIR fluorescence imaging has emerged as an attractive alternative to PET/SPECT and MRI techniques, and may provide a solution for the early diagnosis of AD. In the following sections, we discuss challenges and design strategies associated with the development of NIRF Aβ probes for *in vivo* applications, followed by a list of current reported probes and their optical, binding and brain-kinetic properties, as well as *in vitro* and/or *in vivo* studies (Table 1).

2. Challenges in developing NIRF Aβ probes

A number of NIR fluorophores such as cyanine dyes (Cy7), indocyanine green dyes (ICG), alexa fluor dyes (660–790 nm), and SRfluor dyes have been developed and employed for *in vivo* applications; many of them are commercially available[47]. Nonetheless, these known NIR fluorophores have large molecular weight and intrinsic charges. They are likely to be unsuitable for labeling Aβ plaques in the brain because of their limited BBB permeability. In order to use a fluorophore for *in vivo* brain Aβ imaging, several criteria are required[48–50]: (1) a suitable wavelength of excitation and emission within the NIR range (650−900 nm); (2) high BBB permeability (log*P* values between 2 and 3.5, or *c*log*P*<5.0 are considered optimal[51,52]); (3) high affinity for specific labeling of the Aβ plaques in the brain with low nonspecific binding to other proteins; (4) rapid clearance of the unbound dye from the brain; and (5) significant changes in the probe fluorescence properties upon binding to Aβ plaques. It is challenging to design probes meeting all the requirements. First, many NIR fluorophores are often highly-conjugated structures with molecular weight over 600 Da, while a small and compact scaffold with molecular weight less than 600 Da is required for NIRF Aβ probes. Secondly, the probes should have balanced lipophilicity to ensure good BBB penetration and avoid nonspecific binding. Moreover, high affinity and significant fluorescence property changes require fluorophore scaffolds which are challenging to design. Ultimately, it is difficult to predict *in vivo* properties of a designed NIRF probe before synthesis and testing.

Table 1 Summary of NIR imaging probes for Aβ plaques.

Name	M. W.	K_i (nmol/L)	K_d (nmol/L)	$c\log P$ [a] ($\log P$ [b])	ε (M^{-1} cm^{-1})	λ_{abs} (nm)	λ_{ex} (nm)	λ_{em} (nm) (free)	λ_{em} (nm) (binding)	Φ (%)	Intensity increasement (fold)	References
NIAD-4	334.41	10	–	4.52	35700[c]	–	492[c]	603[c]	–	0.008[d], 5[e,f]	400[f]	48
NIAD-11	400.47	–	–	4.77	–	545[g]	–	690[g]	~710[f]	11[e,f]	–	53
NIAD-16	361.48	–	–	5.33	–	470[g]	–	720[g]	–	–	–	53
AOI-987	324.35	–	220	1.66	61930[i]	650[i]	–	670[i]	–	41[i]	–	49
THK-265	350.37	–	97	−0.29 (1.8)	96198[c]	–	627[c]	644[c]	650	38.5[c]	3.6[f], 6[h]	54
CRANAD-2	410.26	–	38.7	5.56 (3.0)	–	–	640[g]	805[g]	715	0.6[d],40[e,f]	70[c]	50
CRANAD-3	420.55	–	–	5.13	–	–	–	700[g]	640[g]	–	–	55
CRANAD-58	439.31	–	–	5.67 (1.94)	–	–	~630	~750	~700[f]	–	–	56
CRANAD-17	456.25	–	–	5.11	–	–	–	~600	~560[f]	–	–	56
BODIPY7	530.18	108	–	9.08 (2.2)	–	606	–	613	–	36	–	57
BAP-1	351.20	–	44.1	5.47	–	604[j]	614[j]	648[j]	–	46.8[j]	–	58
BAP-2	357.23	–	54.6	5.24	–	651[j]	650[j]	708[j]	–	11.4[j]	–	59
BAP-3	341.16	–	149	4.65	–	665[j]	663[j]	705[j]	–	4.5[j]	–	59
BAP-4	433.32	–	26.8	7.24	–	623[j]	636[j]	704[j]	–	9.3[j]	–	59
BAP-5	417.26	–	18.1	6.75	–	639[j]	649[j]	723[j]	–	4.3[j]	–	59
DANIR 2c	249.31	37	27	2.81	50119[k]	519[k]	597[g]	665[g]	625[h]	4.09[k]	12[h]	60
MAAD-3	327.37	354	–	4.28	–	–	–	704[g]	674 [g,h]	4.71 [d,k] 0.048[d,g]	15[h]	61
DMDAD-3	323.43	645	–	4.36	–	–	–	725[g]	694 [g,h]	2.68 [d,k] 0.033[d,g]	7[h]	61
MCAAD-3	282.34	106	–	3.16	–	–	–	685[g]	654 [g,h]	1.23[d,k] 0.250[d,g]	26[h]	61
DMMAD-3	315.36	652	–	3.53	–	–	–	687[g]	642 [g,h]	0.10 [d,k] 0.068[d,g]	8[h]	61

[a]Calculated using ChemBioDraw 12.0 software.
[b]Experimental value.
[c]Measured in methanol.
[d]Quantum yield before binding.
[e]Quantum yield after binding to Aβ fibrils/aggregates.
[f]For Aβ_{40} fibrils/aggregates.
[g]Measured in PBS.
[h]For Aβ_{42} fibrils/aggregates.
[i]Measured in serum.
[j]Measured in chloroform.
[k]Measured in dichloromethane.

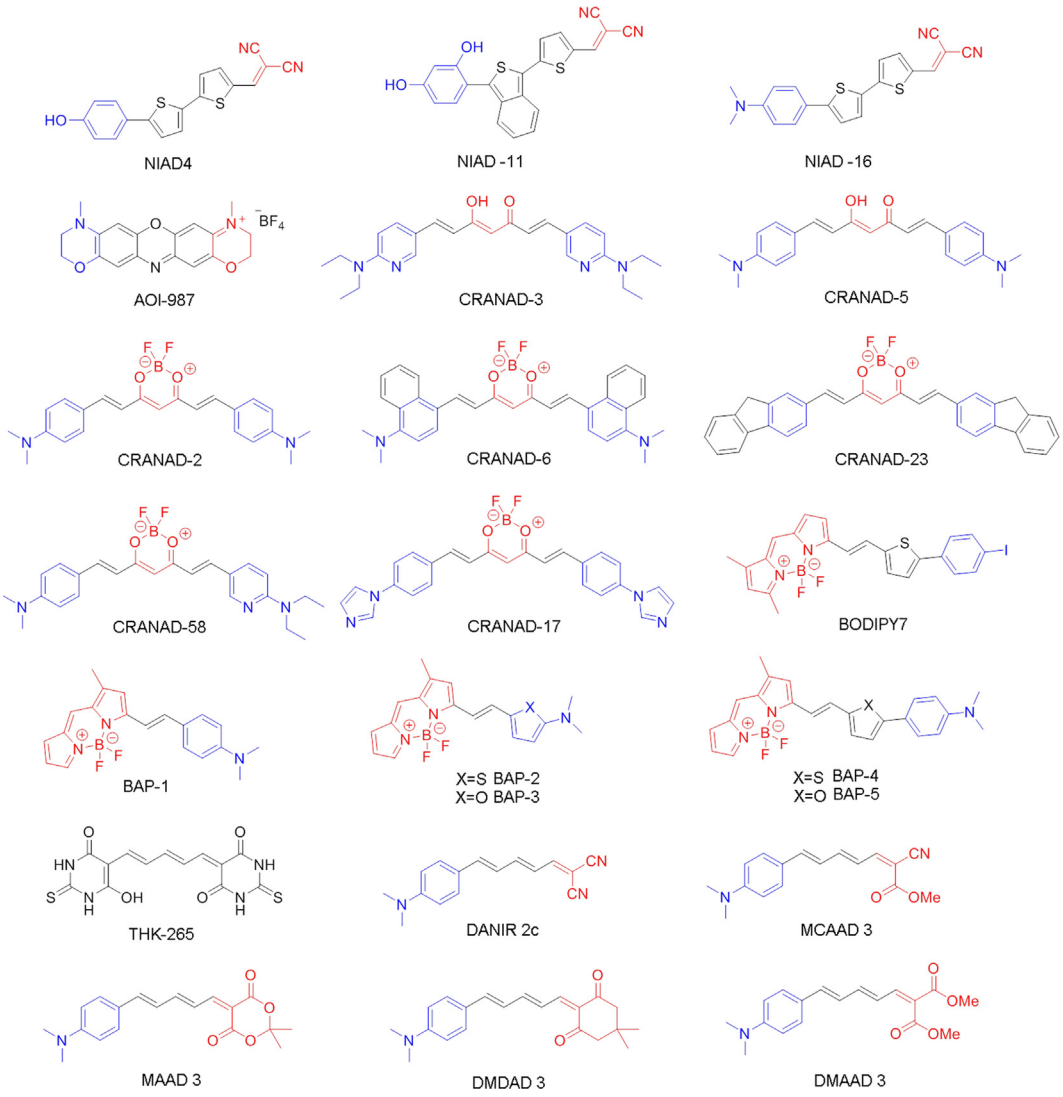

Figure 1 Structures of NIR fluorescence probes covered in this review (donor and acceptor groups were labeled in blue and red, respectively). (For interpretation of the references to color in this figure legend, the reader is referred to the web version of this article.)

3. NIRF Aβ probes

Compared with a vast number of PET/SPECT probes for Aβ plaques in the literature, there have been relatively few reports on the development of NIRF probes. This is no doubt due to the many challenges discussed in the previous section[62]. In this section, we cover six different kinds of NIRF Aβ imaging probes in chronological order according to their publication dates. Their structures are shown in Fig. 1. Most of them are highly conjugated molecules containing the donor-acceptor or donor-acceptor-donor architecture. Their structural features are characterized by an electron-donating group linked to an electron-withdrawing group by an highly polarized conjugated π-electron chain, leading to non-linear optical properties, such as fluorescence intensity change in response to environmental change[63]. Such architecture is particularly useful in the design of NIRF Aβ probes, since the recognition process often involves surrounding environmental changes of the probe[48]. Moreover, physical, optical, and binding properties can be rationally tailored by varying the conjugated π-chain, the donor, and the acceptor groups[48,60,61].

3.1. *NIAD-4 and its analogs (NIAD-4, NIAD-11, and NIAD-16)*

In 2005, Swager et al.[48] rationally designed the fluorescent probe NIAD-4 based upon the donor-π-bridge-acceptor architecture, which utilizes a highly polarizable bisthiophene to link the donor group (*p*-hydroxyphenyl) and the acceptor group (dicyanomethlyene). NIAD-4 showed excellent binding affinity ($K_i = 10$ nmol/L) for Aβ aggregates and a dramatic enhancement of the fluorescence intensity (about 400-fold) when mixing with Aβ aggregates. The increased fluorescence intensity was caused by reduced free rotation of aromatic rings in the excited state. *In vivo* two-photon imaging experiments in transgenic mice demonstrated NIAD-4 readily crossed the BBB after intravenous injection and labeled Aβ plaques in brain and cerebrovascular amyloid angiopathy on blood vessels (Fig. 2)[48]. In a separate study, NIAD-4 showed a broader pH tolerance than Thioflavin T in monitoring amyloid formation process, especially under acidic condition[64]. NIAD-4 presented the first example of the rational design of Aβ specific probes to achieve emission wavelength over 600 nm upon binding with Aβ aggregates. However, the maximum emission wavelength of the probe NIAD-4 is only 603 nm, not in the optimal range of

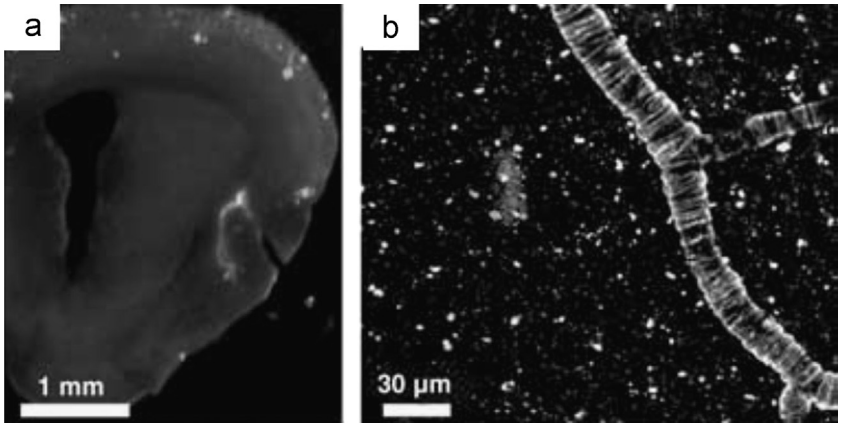

Figure 2 (a) *In vitro* staining of Aβ deposits with NIAD-4 in a coronal section of a transgenic mouse brain. Scale bar, 1 mm. (b) *In vivo* two-photon fluorescent image of Aβ plaques and cerebrovascular amyloid angiopathy. Scale bar, 30 µm. (Adapted with permission from Ref.[48]. Copyright 2005 Wiley-VCH Verlag GmbH & Co. KGaA, Weinheim.)

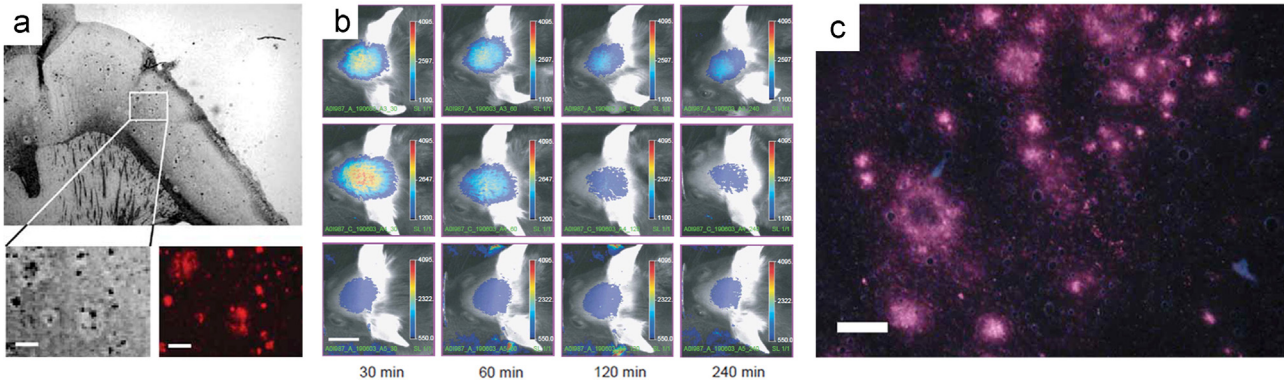

Figure 3 (a) *In vitro* staining of Aβ plaques with AOI-987 in a transgenic mouse brain section [scale bars, 1 mm (large panel) and 100 µm (lower panels)]. (b) *In vivo* images of female 17-month-old APP23 transgenic (top row) and wild-type (middle row) mice at different time points (30, 60, 120, 240 min) after injected *i.v.* with 0.1 mg/kg AOI-987, and corresponding images of a female 17-month-old transgenic APP23 mouse treated with 0.9% saline (bottom row) (scale bar, 1 cm; color scale bars in arbitrary units). (c) *Ex vivo* NIRF image of a brain section (20 µm thickness) of 16-month-old female transgenic mouse administrated with 0.1 mg/kg AOI-987 (scale bar, 100 µmol/L). (Adapted with permission from Ref.[49]. Copyright 2005 Macmillan Publishers Ltd.: Nature Biotechnology.)

650 – 900 nm. Studies with this probe required the use of the invasive cranial window technique to perform *in vivo* fluorescence imaging, which is impractical for clinical diagnosis[48]. To achieve longer emissions, the same group subsequently developed a series of NIAD-4 analogs, including NIAD-11 and NIAD-16[53,65]. NIAD-16 could distinguish vascular and nonvascular Aβ plaques from background signal through fluorescence lifetime imaging[53].

3.2. AOI-987

In the same year, Gremlich et al.[49] at Novartis designed and synthesized longer wavelength benzophenoxazine dyes, as NIRF probes for Aβ plaques. They could monitor the progression of Aβ deposition in APP23 transgenic mice, an animal model of AD. Among them, AOI-987 offered the best *in vivo* results. Although AOI-987 is a charged molecule and has only moderate affinity for Aβ aggregates (K_d = 220 nmol/L), the probe was able to penetrate the BBB and specifically label Aβ plaques as identified by *ex vivo* fluorescence imaging examination of brain slides (Fig. 3c). In addition, AOI-987 has an absorption and emission wavelength within the NIR range (650 and 670 nm, respectively) and a high quantum yield of 0.41. This fulfills the prerequisites for high sensitivity *in vivo* applications. *In vivo* time-dependent NIRF imaging experiments shown in Fig. 3b differentiated APP23 mice from wild type mice in as early as 9 months old. However, AOI-987 has the unfavorable properties of a small Stokes shift (25 nm) and marginal fluorescence changes upon mixing with Aβ aggregates. In addition, the clearance rate of AOI-987 in the brain is low and extended washout time (4 h) is needed to clearly differentiate specific and nonspecific binding *in vivo*[49].

3.3. Curcumin derivatives (CRANAD-2, CRANAD-3, CRANAD-58, CRANAD-17, etc.)

To improve detection signals with noticeable fluorescence intensity alternation and a large Stokes shift, Moore and colleagues[50] designed and synthesized a novel class of NIRF probes derived from curcumin structure. In the structure, a difluoroboronate moiety and two *p*-dimethyamino phenyl groups were integrated into the curcumin scaffold to form a donor-acceptor-donor architecture, significantly increasing the emission wavelength to 805 nm. In this series, CRANAD-2 showed high affinity

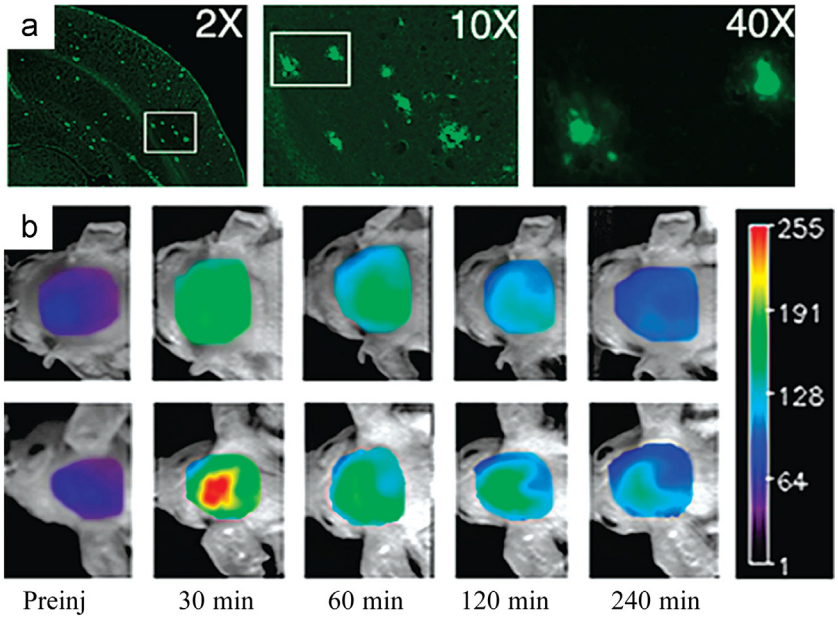

Figure 4 (a) *In vitro* staining of Aβ plaques with CRANAD-2 in a twelve old APP-PS1 transgenic mouse brain section (magnification: left, 2 × ; middle, 10 × ; right, 40 ×). (b) *In vivo* images of female 19-month-old wild type (top row) and Tg2576 (bottom row) mice at different time points (30, 60, 120, 240 min) after injected *i.v.* with 5.0 mg/kg CRANAD-2. (Adapted with permission from Ref.[50]. Copyright 2009 American Chemical Society.)

(K_d = 38.7 nmol/L) and drastic fluorescence changes (70-fold fluorescence intensity increase, 90 nm hypochromic shift) upon binding to Aβ aggregates. Since bulky analogs CRANAD-6 and CRANAD-23 (structures not shown) did not show significant fluorescence change, it was assumed that the binding site of CRANAD-2 is stereo-hindered, likely to be the hydrophobic site containing the core fragment (KLVFF)[56]. *In vitro* staining experiments revealed that CRANAD-2 was capable of selective detection of Aβ plaques in a brain section from a 12-month old APP-PS1 transgenic mouse (Fig. 4a). Notably, CRANAD-2 could differentiate Tg2576 mice from wild type at an early time point (30 min) after injection by comparison of fluorescence intensities in *in vivo* studies (Fig. 4b). CRANAD-2 meets most of the requirements as a NIRF Aβ probe *in vitro* and *in vivo*. Compared with PIB, a well-studied PET probe for Aβ plaques, CRANAD-2 has lower brain entrance/clearance rates[50]. In another study reported by the same group, CRANAD-2 was used in combination with CRANAD-5 as a non-conjugated FRET pair for differentiating Aβ monomers from higher aggregated Aβ species including dimers[66].

By replacing of benzene with pyridine and dimethylamino with diethylamino groups in CRANAD-2, with subsequent removal of the difluoroboron bridge, the same group reported another probe, CRANAD-3, in 2012. CRANAD-3 displayed significant fluorescence property changes upon binding to Aβ aggregates. What was different from CRANAD-2 was that it also interacted with soluble Aβ monomers and dimers, and displayed fluorescence signal change. *In vivo* imaging studies using transgenic APP/PS1 mice exhibited that CRANAD-3 could differentiate 2 month-old APP/PS1 mice from wild type mice. Furthermore, notably, CRANAD-3 could separate specific and nonspecific binding fluorescence signal of the probe in spectral unmixing imaging studies[55].

More recently, new CRANAD-2 analogs were designed and synthesized aiming for NIRF imaging of soluble and insoluble Aβ species and inhibition of copper-ion induced Aβ aggregation[56]. Among them, CRANAD-58 showed different fluorescence response towards soluble and insoluble Aβ species. Significant fluorescence intensity increase (91.9-fold for Aβ_{40}, 113.6-fold for Aβ_{42}) and high affinity (K_d = 105.8 nmol/L for Aβ_{40}, 45.8 nmol/L for Aβ_{42}) for Aβ monomers was observed. Similar fluorescent intensity changes were also seen with Aβ dimers, but to a lesser extent. *In vivo* experiments revealed that CRANAD-58 was able to detect soluble Aβ species in transgenic APP/PS1 mice at the age of 4 months. Another analog, CRANAD-17, containing two copper coordinating imidazoles, could compete and interfere with copper induced crosslinking of Aβ. CRANAD-17 induced 68% more of Aβ monomers as compared with non-treated samples in *in vitro* anti-crosslinking studies, indicating potential usage as theranostic agent[56].

3.4. *BODIPY based probes (BODIPY7, BAP-1 to BAP-5)*

The high quantum yield, biocompatibility, and high lipophilicity of the BODIPY fluorophore render it attractive for the design of NIRF probes. In this regard, inspired by NIAD-4, Ono and his team[57] reported their first BODIPY-derived fluorescence/SPECT dual probe BODIPY7. It contains a conjugated thiophene-phenyl chain similar to NIAD-4. BODIPY7 has modest affinity (K_i = 108 nmol/L) for Aβ aggregates and is able to detect Aβ plaques in *in vitro* staining of brain slides from an animal model of AD. The low BBB permeability, the short absorption/emission wavelength (606/613 nm), and the narrow Stokes shift restricts *in vivo* imaging applications[57]. Two years later, the same group developed a new BODIPY-based Aβ imaging probe (BAP-1) with a "privileged" *p*-dimethylamino phenyl group to improve *in vivo* properties. BAP-1 showed high affinity (K_d = 44.1 nmol/L) and a significant fluorescence intensity increase upon binding to Aβ aggregates. It also has exceptional brain kinetic profiles and demonstrated specific labeling of Aβ plaques based on *in vitro* and *ex vivo* staining studies (Fig. 5). Nonetheless, it failed in *in vivo* imaging

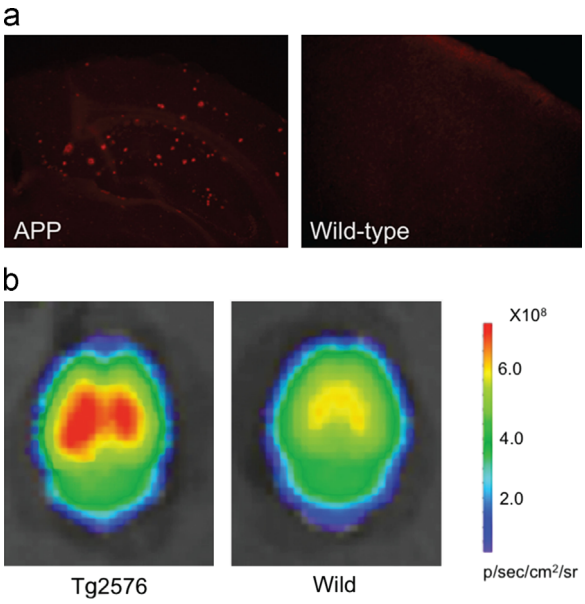

Figure 5 (a) *In vitro* staining of Aβ plaques with BAP-1 in a Tg2576 mouse brain section *versus* a wild-type mouse brain section. (b) Comparison of the *ex vivo* fluorescence intensity in the brain of a 25-month-old Tg2576 and age-matched wild-type mice 1 h after intravenous administration of BAP-1. (Adapted with permission from Ref.[58]. Copyright 2012 American Chemical Society.)

experiments using Tg2576 mice as the disease model, mainly due to unfavorable nonspecific binding in the scalp. Furthermore, the emission wavelength of BAP-1 (648 nm) was still short for *in vivo* imaging[58]. In 2013, several BAP-1 analogs (BAP-2, BAP-3, BAP-4, and BAP-5) with emission wavelength over 700 nm were disclosed. Similar to BAP-1, they were able to selectively label Aβ plaques *in vitro* and *ex vivo*. The probe, BAP-2, was selected for *in vivo* imaging but failed due to the same problem of higher accumulation in the scalp than in the brain, potentially related to high lipophilicity of the BODIPY group[59]. These studies reveal the issues associated with BODIPY-based probes, including narrow Stokes shifts causing potential interference from Raman and Rayleigh scattering, and high lipophilicity leading to nonspecific binding and high background in lipid membranes.

3.5. *THK-265*

Inspired by the reported studies, Okamura and colleagues[54] screened a collection of simple conjugated compounds, which led to the new NIRF Aβ probe, THK-265. This probe possess an emission wavelength around 650 nm combined with favorable physical properties such as high quantum yield, high molar absorption coefficients, and moderate log*P* value. A high binding affinity (K_d = 97 nmol/L) and 6-fold fluorescence intensity increase upon mixing with Aβ_{42} fibrils were observed, albeit no significant change in emission wavelength. THK-265 was further evaluated for its *in vivo* imaging performance using AβPP transgenic mice. Such studies demonstrated that this probe crossed the BBB and selectively labeled Aβ plaques in the brain following intravenous administration. Compared with AOI-987 under the same experimental conditions, THK-265 showed an earlier differentiation time and better imaging contrast between transgenic mice and wild type and higher sensitivity for plaque detection *in vivo*. Most

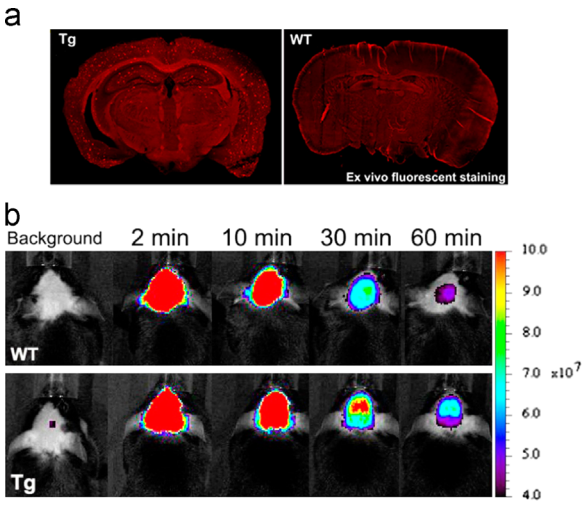

Figure 6 (a) *Ex vivo* image of Aβ plaques in a Tg mouse brain section treated with intravenous administration of 0.4 mg/kg DANIR 2c. (b) *In vivo* images of female 22-month-old wild type (top row) and APPsw/PSEN1 transgenic (bottom row) mice at different time points (2, 10, 30, 60 min) after injected with 0.4 mg/kg DANIR 2c. (Adapted with permission from Ref.[60]. Copyright 2014 American Chemical Society.)

importantly, the fluorescence intensity of THK-265 correlated well with Aβ plaque burden, indicating its potential in monitoring progression of the Aβ aggregation in AD[54]. Subsequently, Schmidt and Pahnke[67] demonstrated that indeed THK-265 could be used for direct monitoring and evaluating different cerebral Aβ aggregation levels in different stage of AD progression in an animal AD model.

3.6. *DANIR 2c and its analogs (MAAD-3, DMDAD-3, MCAAD-3,and DMMAD-3)*

Earlier experiences from previous studies of the BODIPY series of NIRF Aβ probes led to the design of improved ones. By replacement of the undesired BODIPY with simple conjugated systems, Ono and Cui et al.[60] designed and synthesized a new series of structurally simplified Aβ fluorescent probes DANIRs. The *p*-dimethylamino phenyl moiety was used as the donor group on one side of polymethine, with dicyanomethylene as the acceptor on the other end. This design significantly reduced molecular weights of the probes and improved brain kinetics. The best probe in the series, DANIR 2c, was able to efficiently cross the BBB and label Aβ plaques (Fig. 6a) with a fast washout rate of the unbound probe. This probe differentiated between Tg mice and wild type as early as 30 min after *in vivo* administration of the probe (Fig. 6b), a significantly shorter time as compared with that from AOI-987. DANIR 2c also has favorable optical properties (emission wavelength at 665 nm), a 12-fold increase in intensity upon mixing with Aβ aggregates, and excellent affinity for Aβ aggregates (K_i = 37 nmol/L, K_d = 27 nmol/L). DANIR 2c meets most of the requirements as an optimal probe for *in vivo* imaging of Aβ plaques[60]. One shortcoming is the blue-shift of this probe's emission wavelength to only 625 nm (shorter than 650 nm) following binding to Aβ plaques.

Encouraged by the excellent performance of DANIR 2c, Cui et al.[61] then turned to its analogs for better NIRF probes with longer emission wavelength. Four analogs MAAD-3, DMDAD-3,

MCAAD-3, and DMMAD-3 were synthesized, by differing in the donor group. These analogs showed extended emission wavelength and significant reduced binding affinity to Aβ aggregates compared with DANIR 2c. Docking simulations suggested that these probes likely bind to the same binding site as IMPY, which was a thin hydrophobic groove parallel to the fibrillar axis formed by VAL 18 and PHE 20. Increased bulkiness of the acceptor group within these analogs caused a reduced binding efficiency. One analog, MCAAD-3, which had the highest affinity of 106 nmol/L among the series, was selected for *in vivo* imaging studies. Similar to DANIR 2c, MCAAD-3 exhibited good brain kinetics, including rapid initial uptake and fast egress. Furthermore, the latter could differentiate Tg from wild type mice at the earliest point of 30 min after dosing as well. Overall, MCAAD-3 may be a better NIRF probe for *in vivo* imaging than DANIR 2c, as the emission wavelength was at 654 nm when bound to Aβ aggregates.

4. Conclusions

This review highlights the development of NIRF imaging probes for *in vivo* detection of Aβ plaques in the past ten years. Six structurally distinct NIRF fluorophore scaffolds of Aβ probes have been developed. Most of these probes present high affinity for Aβ *in vitro*. As for *in vivo* imaging applications, pharmacokinetics-related properties are as vital as optical properties. Such pharmacokinetics considerations include *in vivo* stability, low-affinity for serum albumin, and reasonable lipophilicity, all of which are required for fast initial uptake into brain and fast washout to reduce nonspecific binding. In addition, significant fluorescence signal changes upon binding to Aβ are required. Other considerations regarding optical properties include absorption/excitation/emission in NIR region, high molar absorption coefficient, high quantum yield, and longer Stokes shifts. The currently reported probes fell short on one or several aspects of these required properties. NIAD-4 and DANIR 2c display a short emission wavelength, but charged AOI-987 is difficult to penetrate the BBB. CRANAD-2 has a slow egress, and BODIPYs suffer from a short Stokes shift and nonspecific binding in the scalp. Marginal fluorescent signal changes are observed with THK-265 upon binding to Aβ aggregates. MCAAD-3 has a relatively lower binding affinity than that of NIAD-4 or DANIR 2c.

Despite these concerns, development of these probes demonstrate the feasibility of NIRF imaging using Aβ specific fluorescence probes as a low-cost, convenient, readily available, and real-time approach for early diagnosis of AD in mice AD models. We believe that, in the future, the NIRF Aβ probes with enhanced pharmacokinetics and optical properties will be great benefits to human health through improved early AD diagnosis, evaluation of disease progression and clinical therapeutic outcomes.

Acknowledgments

The work was supported by the Fundamental Research Funds for the Central Universities and East China University of Science and Technology (start-up funds, Wei Wang), and the China 111 Project (Grant B07023, Wei Wang) is gratefully acknowledged.

References

1. Thies W, Bleiler L, Alzheimer's Association. Alzheimer's disease facts and figures. *Alzheimers Dement* 2013;**9**:208–45.
2. Selkoe DJ. The origins of Alzheimer disease—a is for amyloid. *J Am Med Assoc* 2000;**283**:1615–7.
3. Hamley IW. The amyloid beta peptide: a chemist's perspective. Role in Alzheimer's and fibrillization. *Chem Rev* 2012;**112**:5147–92.
4. Savelieff MG, DeToma AS, Derrick JS, Lim MH. The ongoing search for small molecules to study metal-associated amyloid-β species in Alzheimer's disease. *Acc Chem Res* 2014;**47**:2475–82.
5. Hardy JA, Higgins GA. Alzheimer's disease: the amyloid cascade hypothesis. *Science* 1992;**256**:184–5.
6. Hardy J, Selkoe DJ. The amyloid hypothesis of Alzheimer's disease: progress and problems on the road to therapeutics. *Science* 2002;**297**:353–6.
7. Kepp KP. Bioinorganic chemistry of Alzheimer's disease. *Chem Rev* 2012;**112**:5193–239.
8. Rauk A. The chemistry of Alzheimer's disease. *Chem Soc Rev* 2009;**38**:2698–715.
9. Kung HF. The β-amyloid hypothesis in Alzheimer's disease: seeing is believing. *ACS Med Chem Lett* 2012;**3**:265–7.
10. Poduslo JF, Wengenack TM, Curran GL, Wisniewski T, Sigurdsson EM, Macura SI, et al. Molecular targeting of Alzheimer's amyloid plaques for contrast-enhanced magnetic resonance imaging. *Neurobiol Dis* 2002;**11**:315–29.
11. Flaherty DP, Walsh SM, Kiyota T, Dong Y, Ikezu T, Vennerstrom JL. Polyfluorinated bis-styrylbenzene β-amyloid plaque binding ligands. *J Med Chem* 2007;**50**:4986–92.
12. Li S, He H, Cui W, Gu B, Li J, Qi Z, et al. Detection of Aβ plaques by a novel specific MRI probe precursor CR-BSA-(Gd-DTPA)$_n$ in APP/PS1 transgenic mice. *Anat Rec* 2010;**293**:2136–43.
13. Martins AF, Morfin JF, Kubíčková A, Kubíček V, Buron F, Suzenet F, et al. PiB-conjugated, metal-based imaging probes: multimodal approaches for the visualization of β-amyloid plaques. *ACS Med Chem Lett* 2013;**4**:436–40.
14. Sun WG, Li HH. Application of MRI molecular probes in the diagnosis of Alzheimer's disease. *Prog Anat Sci* 2013;**19**:464–6.
15. Rowe CC, Villemagne VL. Brain amyloid imaging. *J Nucl Med Technol* 2013;**41**:11–8.
16. Mathis CA, Mason NS, Lopresti BJ, Klunk WE. Development of positron emission tomography β-amyloid plaque imaging agents. *Semin Nucl Med* 2012;**42**:423–32.
17. Koo JH, Byun Y. Current status of PET-imaging probes of β-amyloid plaques. *Arch Pharm Res* 2013;**36**:1178–84.
18. Zhu L, Ploessl K, Kung HF. PET/SPECT imaging agents for neurodegenerative diseases. *Chem Soc Rev* 2014;**43**:6683–91.
19. Henriksen G, Yousefi BH, Drzezga A, Wester HJ. Development and evaluation of compounds for imaging of β-amyloid plaque by means of positron emission tomography. *Eur J Nucl Med Mol Imag* 2008;**35 Suppl 1**:S75–81.
20. Zhuang ZP, Kung MP, Wilson A, Lee CW, Plössl K, Hou C, et al. Structure–activity relationship of imidazo[1,2-*a*]pyridines as ligands for detecting β-amyloid plaques in the brain. *J Med Chem* 2003;**46**:237–43.
21. Bois F, Baldwin RM, Amici L, Al-Tikriti MS, Kula N, Baldessarini R, et al. Synthesis, radiolabeling, and baboon SPECT imaging of 2β-carbomethoxy-3β-(3'-[^{123}I]iodophenyl)tropane ([^{123}I]YP256) as a serotonin transporter radiotracer ([^{123}I]YP256) a potential serotonin transporter radiotracer). *Nucl Med Biol* 2008;**35**:53–9.
22. Watanabe H, Ono M, Kimura H, Kagawa S, Nishii R, Fuchigami T, et al. A dual fluorinated and iodinated radiotracer for PET and SPECT imaging of β-amyloid plaques in the brain. *Bioorg Med Chem Lett* 2011;**21**:6519–22.
23. Cheng Y, Ono M, Kimura H, Ueda M, Saji H. Technetium-99 m labeled pyridyl benzofuran derivatives as single photon emission computed tomography imaging probes for β-amyloid plaques in Alzheimer's brains. *J Med Chem* 2012;**55**:2279–86.
24. Yang Y, Cui M, Jin B, Wang XD, Li ZJ, Yu PR, et al. ^{99m}Tc-labeled dibenzylideneacetone derivatives as potential SPECT probes for *in vivo* imaging of β-amyloid plaque. *Eur J Med Chem* 2013;**64**:90–8.

25. Zhang XL, Ran CZ. Dual functional small molecule probes as fluorophore and ligand for misfolding proteins. *Curr Org Chem* 2013;**17**:580–93.
26. Golde TE, Bacskai BJ. Bringing amyloid into focus. *Nat Biotechnol* 2005;**23**:552–4.
27. Mathis CA, Wang YM, Holt DP, Huang GF, Debnath ML, Klunk WE. Synthesis and evaluation of ^{11}C-labeled 6-substituted 2-arylbenzothiazoles as amyloid imaging agents. *J Med Chem* 2003;**46**:2740–54.
28. Klunk WE, Engler H, Nordberg A, Wang Y, Blomqvist G, Holt DP, et al. Imaging brain amyloid in Alzheimer's disease with Pittsburgh Compound-B. *Ann Neurol* 2004;**55**:306–19.
29. Ono M, Wilson A, Nobrega J, Westaway D, Verhoeff P, Zhuang ZP, et al. ^{11}C-labeled stilbene derivatives as Aβ-aggregate-specific PET imaging agents for Alzheimer's disease. *Nucl Med Biol* 2003;**30**:565–71.
30. Verhoeff N, Wilson AA, Takeshita S, Trop L, Hussey D, Singh K, et al. *In-vivo* imaging of Alzheimer disease β-amyloid with [^{11}C]SB-13 PET. *Am J Geriatr Psychiatry* 2004;**12**:584–95.
31. Johnson AE, Jeppsson F, Sandell J, Wensbo D, Neelissen JA, Juréus A, et al. AZD2184: a radioligand for sensitive detection of β-amyloid deposits. *J Neurochem* 2009;**108**:1177–86.
32. Vandenberghe R, van Laere K, Ivanoiu A, Salmon E, Bastin C, Triau E, et al. ^{18}F-flutemetamol amyloid imaging in Alzheimer disease and mild cognitive impairment: a phase 2 trial. *Ann Neurol* 2010;**68**:319–29.
33. Juréus A, Swahn BM, Sandell J, Jeppsson F, Johnson AE, Johnström P, et al. Characterization of AZD4694, a novel fluorinated Aβ plaque neuroimaging PET radioligand. *J Neurochem* 2010;**114**:784–94.
34. Cselényi Z, Jönhagen ME, Forsberg A, Halldin C, Julin P, Schou M, et al. Clinical validation of ^{18}F-AZD4694, an amyloid-β-specific PET radioligand. *J Nucl Med* 2012;**53**:415–24.
35. Agdeppa ED, Kepe V, Liu J, Flores-Torres S, Satyamurthy N, Petric A, et al. Binding characteristics of radiofluorinated 6-dialkylamino-2-naphthylethylidene derivatives as positron emission tomography imaging probes for β-amyloid plaques in Alzheimer's disease. *J Neurosci* 2001;**21**:RC189.
36. Shoghi-Jadid K, Small GW, Agdeppa ED, Kepe V, Ercoli LM, Siddarth P, et al. Localization of neurofibrillary tangles and β-amyloid plaques in the brains of living patients with Alzheimer disease. *Am J Geriatr Psychiatry* 2002;**10**:24–35.
37. Zhang W, Oya S, Kung MP, Hou C, Maier DL, Kung HF. F-18 polyethyleneglycol stilbenes as PET imaging agents targeting Aβ aggregates in the brain. *Nucl Med Biol* 2005;**32**:799–809.
38. Rowe CC, Ackerman U, Browne W, Mulligan R, Pike KL, O'Keefe G, et al. Imaging of amyloid β in Alzheimer's disease with ^{18}F-BAY94-9172, a novel PET tracer: proof of mechanism. *Lancet Neurol* 2008;**7**:129–35.
39. Barthel H, Gertz HJ, Dresel S, Peters O, Bartenstein P, Buerger K, et al. Cerebral amyloid-β PET with florbetaben (^{18}F) in patients with Alzheimer's disease and healthy controls: a multicentre phase 2 diagnostic study. *Lancet Neurol* 2011;**10**:424–35.
40. Zhang W, Kung MP, Oya S, Hou C, Kung HF. ^{18}F-labeled styrylpyridines as PET agents for amyloid plaque imaging. *Nucl Med Biol* 2007;**34**:89–97.
41. Choi SR, Golding G, Zhuang Z, Zhang W, Lim N, Hefti F, et al. Preclinical properties of ^{18}F-AV-45: a PET agent for Aβ plaques in the brain. *J Nucl Med* 2009;**50**:1887–94.
42. Wong DF, Rosenberg PB, Zhou Y, et al. *In vivo* imaging of amyloid deposition in Alzheimer disease using the radioligand ^{18}F-AV-45 (florbetapir [corrected] F 18). *J Nucl Med* 2010;**51**:913–20.
43. Williams SCP. Alzheimer's imaging agents struggle to find a market outside trials. *Nat Med* 2013;**19**:1551.
44. Ntziachristos V, Bremer C, Weissleder R. Fluorescence imaging with near-infrared light: new technological advances that enable *in vivo* molecular imaging. *Eur Radiol* 2003;**13**:195–208.
45. Ntziachristos V. Fluorescence molecular imaging. *Annu Rev Biomed Eng* 2006;**8**:1–33.
46. Frangioni JV. *In vivo* near-infrared fluorescence imaging. *Curr Opin Chem Biol* 2003;**7**:626–34.
47. Licha K, Olbrich C. Optical imaging in drug discovery and diagnostic applications. *Adv Drug Deliv Rev* 2005;**57**:1087–108.
48. Nesterov EE, Skoch J, Hyman BT, Klunk WE, Bacskai BJ, Swager TM. *In vivo* optical imaging of amyloid aggregates in brain: design of fluorescent markers. *Angew Chem Int Ed Engl* 2005;**44**:5452–6.
49. Hintersteiner M, Enz A, Frey P, Jaton AL, Kinzy W, Kneuer R, et al. *In vivo* detection of amyloid-β deposits by near-infrared imaging using an oxazine-derivative probe. *Nat Biotechnol* 2005;**23**:577–83.
50. Ran C, Xu X, Raymond SB, Ferrara BJ, Neal K, Bacskai BJ, et al. Design, synthesis, and testing of difluoroboron-derivatized curcumins as near-infrared probes for *in vivo* detection of amyloid-β deposits. *J Am Chem Soc* 2009;**131**:15257–61.
51. Ametamey SM, Honer M, Schubiger PA. Molecular imaging with PET. *Chem Rev* 2008;**108**:1501–16.
52. Clark DE. Computational prediction of blood-brain barrier permeation. In Doherty A, editor. *Annual reports in medicinal chemistry*, San Diego: Elsevier Academic Press; 2005. p, 403–15.
53. Raymond SB, Skoch J, Hills ID, Nesterov EE, Swager TM, Bacskai BJ. Smart optical probes for near-infrared fluorescence imaging of Alzheimer's disease pathology. *Eur J Nucl Med Mol Imaging* 2008;**35 Suppl 1**:S93–8.
54. Okamura N, Mori M, Furumoto S, Yoshikawa T, Harada R, Ito S, et al. *In vivo* detection of amyloid plaques in the mouse brain using the near-infrared fluorescence probe THK-265. *J Alzheimers Dis* 2011;**23**:37–48.
55. Ran C, Moore A. Spectral unmixing imaging of wavelength-responsive fluorescent probes: an application for the real-time report of amyloid β species in Alzheimer's disease. *Mol Imaging Biol* 2012;**14**:293–300.
56. Zhang XL, Tian YL, Li Z, Tian XY, Sun HB, Liu H, et al. Design and synthesis of curcumin analogues for *in vivo* fluorescence imaging and inhibiting copper-induced cross-linking of amyloid β species in Alzheimer's disease. *J Am Chem Soc* 2013;**135**:16397–409.
57. Ono M, Ishikawa M, Kimura H, Hayashi S, Matsumura K, Watanabe H, et al. Development of dual functional SPECT/fluorescent probes for imaging cerebral β-amyloid plaques. *Bioorg Med Chem Lett* 2010;**20**:3885–8.
58. Ono M, Watanabe H, Kimura H, Saji H. BODIPY-based molecular probe for imaging of cerebral β-amyloid plaques. *ACS Chem Neurosci* 2012;**3**:319–24.
59. Watanabe H, Ono M, Matsumura K, Yoshimura M, Kimura H, Saji H. Molecular imaging of β-amyloid plaques with near-infrared boron dipyrromethane (BODIPY)-based fluorescent probes. *Mol Imaging* 2013;**12**:338–47.
60. Cui MC, Ono M, Watanabe H, Kimura H, Liu BL, Saji H. Smart near-infrared fluorescence probes with donor-acceptor structure for *in vivo* detection of β-amyloid deposits. *J Am Chem Soc* 2014;**136**:3388–94.
61. Fu H, Cui M, Tu P, Pan Z, Liu B. Evaluation of molecules based on the electron donor–acceptor architecture as near-infrared β-amyloidal-targeting probes. *Chem Commun* 2014;**50**:11875–8.
62. Cui MC. Past and recent progress of molecular imaging probes for β-amyloid plaques in the brain. *Curr Med Chem* 2014;**21**:82–112.
63. Meyers F, Marder SR, Pierce BM, Bredas JL. Electric-field modulated nonlinear-optical properties of donor-acceptor polyenes: sum-over-states investigation of the relationship between molecular polarizabilities (α, β and γ) and bond-length alternation. *J Am Chem Soc* 1994;**116**:10703–14.
64. Brandenburg E, von Berlepsch H, Koksch B. Specific *in situ* discrimination of amyloid fibrils *versus* α-helical fibres by the fluorophore NIAD-4. *Mol BioSyst* 2012;**8**:557–64.
65. Meek ST, Nesterov EE, Swager TM. Near-infrared fluorophores containing benzo[*c*]heterocycle subunits. *Org Lett* 2008;**10**:2991–3.
66. Ran CZ, Zhao W, Moir RD, Moore A. Non-conjugated small molecule FRET for differentiating monomers from higher molecular weight amyloid β species. *PLoS One* 2011;**6**:e19362.
67. Schmidt A, Pahnke J. Efficient near-infrared *in vivo* imaging of amyoid-β deposits in Alzheimer's disease mouse models. *J Alzheimers Dis* 2012;**30**:651–64.